Available online at www.sciencedirect.com
SCIENCE DIRECT®
Biochemical and Biophysical Research Communications 332 (2005) 109–116
BBRC
www.elsevier.com/locate/ybbrc

Detection of nanometer-sized particles in living cells using modern fluorescence fluctuation methods

Michael Edetsberger [a,*,1], Erwin Gaubitzer [a,1], Eva Valic [b], Elisabeth Waigmann [c], Gottfried Köhler [a]

[a] Max F. Perutz Laboratories, Department of Chemistry, University of Vienna, Campus-Vienna-Biocenter 5, A-1030 Vienna, Austria
[b] Allgemeine Unfallversicherungs-Anstalt, AUVA, Aldalbert-Stifterstrasse 65, A-1201 Vienna, Austria
[c] Max F. Perutz Laboratories, University Departments at the Vienna Biocenter, Department of Medical Biochemistry, Medical University of Vienna, Dr. Bohrgasse 9, A-1030 Vienna, Austria

Received 13 April 2005
Available online 27 April 2005

Abstract

Nanosized materials are increasingly used in medicine and biotechnology but originate also from various aerosol sources. A detailed understanding of their interaction with cells is a prerequisite for specific applications and appraisal of hazardous effects. Fluorescence fluctuation methods are applied to follow the time-course of the translocation and distribution of fluorescent 20 nm polystyrene nanoparticles with negative surface charges in HeLa cells under almost physiological conditions. The experimental results demonstrate that singular particles enter the cell without significant contribution by endocytotic mechanisms and are distributed within the cytoplasm. Subsequently aggregation is observed, which can be blocked by cytotoxins, like Genistein and Cytochalasin B, interfering with cellular uptake processes. The observed non-active uptake is due to non-specific interactions with the cell surface and could be responsible for distribution of nanometer-sized materials in tissue.

Keywords: Nanoparticles; Laser scanning microscope; Fluorescence correlation spectroscopy; Photon counting histogramming; Auto correlation function; Fluorescence intensity distribution analysis

Nanoparticles are small minute parts appearing dispersed in fluid or gaseous media. Common size limits are: particles up to 50 nm in diameter are called nanoparticles, and between 50 and 100 nm ultrafine particles [1].

Nanometer sized particles like fullerenes [2], quantum dots [3], particulate drug delivery systems, and Dendrosomes as DNA carrier [4] are discussed due to their novel and unique properties for application in life sciences and medical treatment. Nevertheless, possible negative health effects became an issue in environmental sciences as nanoparticulate matter appears also in ambient air as a result of a variety of technological processes. Especially the $PM_{2.5}$[2] fraction of these emissions, which consist mainly of carbon associated with metals, oxygen, and organic matter, is assumed to threaten public health [5] and even heritable effects are possible [1,6].

Nanoparticles and ultrafine particles are also an issue in job safety and therefore global research activities are focused on different kinds of aerosol sources, such as coal fly ash [7] and diesel exhaust particles [8] from modern combustion and fabrication processes. Exposed workers (e.g., road- or tunnel construction-sites) carry

* Corresponding author. Fax: +43 1 4277 9522.
E-mail addresses: michael.edetsberger@univie.ac.at (M. Edetsberger), erwin.gaubitzer@univie.ac.at (E. Gaubitzer).
[1] These two authors contributed equally.

[2] Denotes particle matter (PM) smaller than 2.5 μm in diameter.

0006-291X/$ - see front matter © 2005 Elsevier Inc. All rights reserved.
doi:10.1016/j.bbrc.2005.04.100

an incalculable risk to contract physiological sequels due to the exposure.

Cells of the alimentary canal, the urogenital tract, the lung, and the skin are exposed to the ambient environment. Whereas the skin builds up a physical barrier, the cells of the lung, different varieties of the epithelium, and the intestinal tract deal with matter transport. In general, the lung of mammals can be regarded as a filter system. In the upper respiratory tract, bigger particles deposit on cilia and are removed by sputum. Dust particles from technical processes might be a hundred times smaller than natural dust and are therefore able to penetrate into the bronchioles and the alveolar region. Within the alveolae the air is virtually stagnant and therefore diffusion becomes decisive for the further translocation into the bloodstream and the lymphatic system. Studies with intravenously injected ultrafine particles have shown that the liver is the major organ of accumulation [9] but they were also found in tumor cells and tumor-associated macrophages of rodents [10] and carbon nanoparticles were even found in brains of rats [11].

Particles up to 200 nm in diameter are able to enter cells without an active uptake process. This unspecific uptake was shown for different cell lines using confocal laser scanning microscopy (LSM), transmission electron microscopy, and electron energy-loss spectroscopy [12,13]. Such techniques provide information about the spatial distribution, shape, and size of particles within fixed or at least pre-experimentally treated cells. In contrast, the rather new combination of confocal microscopy based fluorescence fluctuation methods like fluorescence correlation spectroscopy (FCS) [14] and fluorescence intensity distribution analysis (FIDA) [15] allows us to get informations about size and dynamic properties of particles in the cytoplasm also of untreated cells.

FCS uses the auto correlation function (ACF) of fluorescent particles diffusing through the focus volume (10^{-18} m^3=1 fL) to extract their number and diffusion coefficient. FIDA uses the photon counting histogram (PCH) [16] to extract molecular brightness which can be seen as a direct parameter for the size of particles [17]. We applied these methods to follow the time-course of the uptake of fluorescent particles into living cells.

The contribution of endocytotic processes to the mechanism of their translocation was analyzed using two cytotoxins. The tyrosine kinase inhibitor Genistein, which is known to inhibit endocytotic mechanisms, especially caveolae internalization [18], the recruitment of different receptors in clathrin-coated pits [19], and the routing from early endosomes in lysosomes [20], and the cell permeable fungal toxin Cytochalasin B, which interacts with actin polymerization [21] and disrupts various cell processes.

The main aim of this study was to detect fluorescent particles in living cells. We discriminated particles and different aggregates within the cell and determined their dynamic properties and the time-course of their appearance in the cytoplasm. LSM was used to complete the measured data.

Materials and methods

Cell culture. Cell culture reagents were obtained from Sigma–Aldrich (Austria) and Euroclone (Austria), Genistein, and Cytochalasin B were from Sigma–Aldrich (Austria).

HeLa cells-human cervix carcinoma cells. HeLa cells (OHIO cell line ATCC, provided by the Medical University Vienna) were routinely cultured in DMEM (high glucose −4500 mg glucose) containing 4.5 mM L-glutamine, 44 mM Na-bicarbonate, 100 U/ml penicillin, 100 μg/ml streptomycin, 0.9 mM Na-pyruvate, and 10% fetal calf serum in a 6% CO_2 humidified atmosphere at 37 °C (standard conditions).

Preparation for LSM. HeLa cells (1×10^4 cells/ml) were seeded on coverslips (Assistent, Germany) in 35 mm tissue wells (IWAKI, Japan) and grown overnight at standard conditions. Cells were washed twice with PBS containing 20 mM glucose (PBSG, pH 7.4) at 37 °C. Then the cells were stained with 10 μM Nile-Red for 20 min at 37 °C. For imaging the cells were incubated with 0.018%(w/w) 20 nm, carboxy-coated, green fluorescent polystyrene particles (Fluospheres, Molecular Probes) in PBSG.

Preparation for FCS and PCH. Cells (3×10^4 cells/ml) were seeded in 8-well LabTek chambered slides (NUNC) and grown overnight at standard conditions. Cells were washed twice with PBSG at 37 °C. Then the cells were submerged with PBSG at 37 °C. For measuring FCS and PCH the cells were incubated with 0.005%(w/w) 20 nm, carboxy coated, green fluorescent polystyrene particles (Fluospheres, Molecular Probes) in 0.4% trypan blue solution (Sigma–Aldrich) to block signals from outside the cell [12]. Measurements started immediately after adding the particles.

Blocking of uptake (LSM, FCS, and PCH). After growing the cells overnight the culture medium was removed by new medium (DMEM) containing 200 mM Genistein [12] or 10 μM Cytochalasin B [22]. Cells were incubated for 60 min under standard conditions and afterwards washed twice with PBSG (37 °C). The further treatments were performed in the same way as for untreated samples.

Setup for LSM. Live cell confocal images were performed using a confocal laser scanning microscope (Leica SP1, Germany), a CW Ar^+ laser, and an oil immersion objective (PL APO 100×1.4 oil UV). Images for the fluorescent particles were performed using the laser line at $\lambda_{exc} = 488$ nm and detected by a photo-multiplier tube (PMT) in the range of 500–540 nm (green channel; setup 1, HV710/offset 0.39; setup 2, HV 739/offset 1.17). Images for the stained cells were performed using the laser line at $\lambda_{exc} = 568$ nm and detected by a PMT in the range of 580–640 nm (red channel; setup 1, HV594/offset 0.39; setup 2, HV 756/offset 1.17). Images of cells treated with Genistein (with or without particles added) were performed with setup 1 and images of untreated cells (particles added) were performed with setup 2. Imaging started 20 min after adding the particles and all images were averages of three individual scans. Images were extracted and overlays were performed using the Leica Simulator Software (Leica, Germany) or Adobe Photoshop 6.0.

Setup for FCS and PCH. Measurements were performed using a ConfoCor1 (Carl Zeiss, Jena, Germany), an Ar^+ laser (Lasos, Germany; $\lambda = 488$ nm, 0.3 mW/cm^2), a water immersion objective (Zeiss, C-Apochromat 63×, 1.2 W corr) and an Avalanche Photo-Diode (APD, Perkin-Elmer SPCM-AQR-13-FC). Confocal pinhole diameter was set to 35 μm and calibrated with rhodamine-6 G (R6G, diffusion constant: 2.8×10^{-6} cm^2/s; diffusion time: 0.03 ms). Fluorescence was detected through a dichroic mirror (>510 nm) and a band-pass filter (520–570 nm).

FCS analysis. Fluorescence signals were detected for 42 s with 3 s interval and 12 s correlator scaling. The autocorrelation ($G(\tau)$) was fitted using FCS Access version 1.0.12 (Evotec, Germany) applying a structural parameter SP = (1/2 × focus length)/focus radius of 5.6 obtained from the measurement with R6G according to the following formula [23]:

$$G(\tau) = \frac{\langle \delta I(t)\delta I(t+\tau)\rangle}{\langle \delta I(t)\rangle^2} = 1 + \frac{1}{N}\sum_{i=1\ldots3}\frac{F_i}{(1+\frac{\tau}{\tau_i})}\frac{1}{\sqrt{(1+\frac{\tau}{SP^2\tau_i})}}. \quad (1)$$

F_i and τ_i are the fraction and diffusion time of component i, respectively, and N represents the number of particles in the focus element. The term δI denotes the deviation of intensity from the temporal average. From the diffusion-constant (D_{R6G}) and the diffusion-time (τ_{R6G}) of R6G and knowing diffusion times of particles ($\tau_{particles}$) their hydrodynamic radii ($r_{hydrodynamic}$) can be obtained [23]:

$$r_{hydrodynamic} = \frac{kT\tau_{particles}}{96D_{R6G}\tau_{R6G}\pi\eta}. \quad (2)$$

Here k denotes the Boltzmann constant, T stands for the absolute temperature, and η represents the viscosity of the cytoplasm (2.2 cp) [24].

PCH analysis. To obtain raw data, fluorescence signals were detected using a Time Measurement Histogram Accumulating Real-Time Processor (PC Board for Time Correlated Single Photon Counting, Time Harp 100, PicoQuant, Software version 3.0) triggered with 7.4 MHz. The histogram of counted photons is acquired by monitoring the signal intensity during 30 s and plotting the numbers of photons detected in a time window (t_{40}) of 40 μs. The values were analyzed using the generating function [25]:

$$G(\xi) = \exp\left[(\xi-1)\lambda t_{40} + \sum_s c_s \int_V e^{\{[(\xi-1)q_s t_{40}B(r)]-1\}} dV\right]. \quad (3)$$

Here, c_s relates to the concentration and q_s accounts for the specific brightness of different particle species (s). The term λ is a parameter for background noise and $B(r)$ represents the spatial brightness distribution in the focal volume (V). After calculation of $G(\xi)$, the probability distribution is retrieved by an inverse Fourier transformation:

$$P(n, t_{40}) = FFT^{-1}G(\xi, t_{40}). \quad (4)$$

Raw data recorded with Time Harp 100 were histogrammed and normalized by area. The resulting data were fitted using a modified Levenberg–Marquardt least squares algorithm. All software was written in the Python programming language. All graphs were drawn using Origin 6.1 (Origin Lab, USA).

Results

Laser scanning microscopy

HeLa cells were imaged before and after a pre-treatment with Genistein (compilation in Fig. 1). HeLa cells, treated with Genistein, stained with Nile-Red but not incubated with green fluorescent particles showed a clear image in the red detection channel but a weak signal in the green channel (Fig. 1A). Cells stained with Nile-Red and incubated with particles showed images in both channels (Figs. 1B and C). In the sample treated with Genistein the diffuse green fluorescence of mainly isolated particles was observed, which became apparent by the image in the green channel. Only small aggregates, which can be identified as green spots, appeared sporadically at the very peripheric region of the cell (Fig. 1B). In the untreated sample mainly isolated particles (diffuse green fluorescence) and very small aggregates (seen as green spots) were observed. These species of particles were found all over the cell. Additionally very big and bright aggregates (yellow spots) of different size were observed. The yellow color is a result of the overlay of the green and red images indicating that these aggregated particles were mainly found at stainable structures in the cytoplasm. Yellow structures which seem to be in the nucleus are residual signals from the section above the nucleus (Fig. 1C). Nevertheless, it is necessary to have viable cells and a fluid membrane, because in dead cells no translocation of particles could be observed. In that case, the particles were just attached to the outside of the cell membrane (picture not shown).

FCS measurement

The diffusion behavior of green fluorescent particles was measured in the cytoplasm of untreated HeLa cells and HeLa cells treated with Genistein or Cytochalasin B (Fig. 2).

The resulting autocorrelation curves were analyzed using a multiple-component model. After adding particles to the submerged cells, the fluorescence signal in the cytoplasm increased. As there was generally a delay of about 1 min between the addition and the first measurement, a clear fluorescence intensity was already recorded from the interior of the cell. This indicates that the translocation of the particles into the cell occurred without delay. The intensity was dependent on the concentration of particles, its sedimentation properties, and the selected cell. Therefore, different initial signal intensities could be detected in individual measurements (representative results see Fig. 2).

Only at low intensities, i.e., low particle concentrations, the measured intensity fluctuations were large enough to extract diffusion parameters. A typical measurement for untreated cells is shown in Figs. 2A1 and A2. The measurement of cells treated with Genistein or Cytochalasin B showed already much higher initial intensities and thus only small fluctuations. At particle concentrations frequently observed during experiments, the fluorescence intensities were above 100 kHz and correlations were often lost. Analysis of the autocorrelation curves at early time-points after addition of particles gave a mean value of 1.0 ± 0.3 ms for the diffusion time. Applying Eq. 2 (see Materials and methods) a hydrodynamic radius of 14 ± 4 nm was obtained. This value is in agreement with the mean diameter of about 20 nm of individual particles (Species 1). The loss of any correlation at later time-points was the result of a too high particle concentration in the observed cell. Over a period of about 10 min the signal intensity passed through a maximum value and stabilized at a slightly lower intensity, dependent on the initial particle concentration but inde-

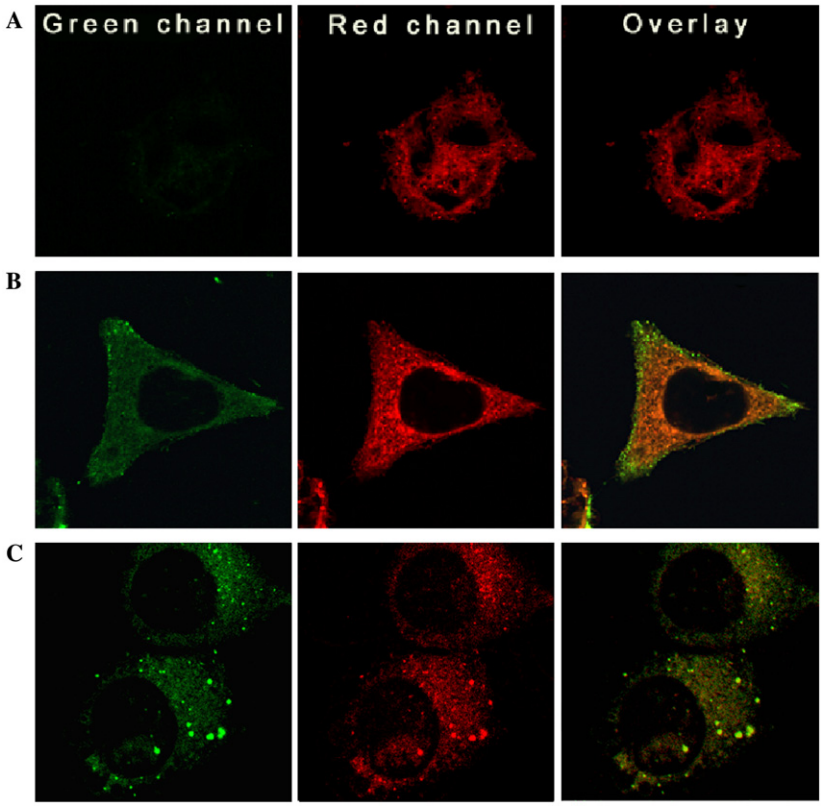

Fig. 1. Confocal images of HeLa cells. (A) HeLa cells stained with Nile-Red and treated with Genistein. (B) HeLa cells stained with Nile-Red, treated with Genistein, and incubated with green fluorescent particles. (C) Native HeLa cells stained with Nile-Red and incubated with green fluorescent particles. Images represent sections of 500 nm thickness taken 3–4 μm above the glass surface. (For interpretation of the references to colors in this figure legend, the reader is referred to the web version of this paper.)

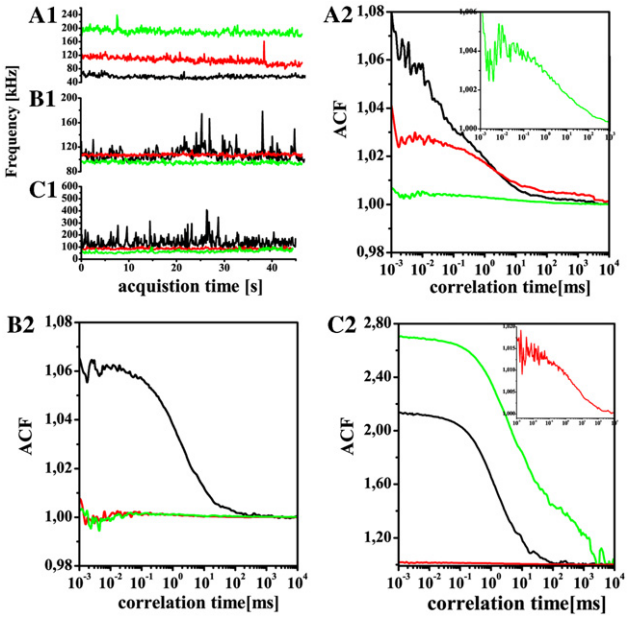

Fig. 2. Fluorescence correlation measurements in HeLa cells. (A1–C1) Intensity scans measured at different time-points. (A2–C2) Auto correlation function (ACF) obtained at different time-points. Untreated cells (black), cells treated with Genistein (red) and Cytochalasin B (green). (For interpretation of the references to colors in this figure legend, the reader is referred to the web version of this paper.)

pendent of whether the cell was treated with cytotoxins or not.

About 10–15 min after addition of particles, the picture changed dramatically (see Figs. 2B1 and B2). Whereas in untreated cells high fluorescence fluctuations occurred this was not the case for treated cells. Here a two component model had to be applied resulting in diffusion times of 1.3 ± 0.4 and 7 ± 1 ms. The first value indicates Species 1 whereas the second value can be attributed to clusters of a large number of particles. A radius of 102 ± 14 nm was obtained for this bright species (Species 2). During the next 20 min, no correlation could be found in cells treated with Genistein or Cytochalasin B.

Additional effects occurred after 40 min which were observed for the next 20 min. In the untreated cells, intensities did not change significantly, but an additional species with a diffusion time of 35 ± 11 ms appeared (for 60 min of incubation see C1 and C2, Fig. 2). This species with a radius larger than 350 nm was not seen in any of the drug treated samples. However, larger intensity fluctuations were also observed in the drug treated samples (see Figs. 2C1 and C2) but contributing much less to the overall fluorescence intensity than in untreated cells. Diffusion times between 6 and 21 ms, similar to those

Table 1
Average size distribution and relations of detected species

Incubation time (min)	Species 1		Species 2		Species 3	
	$r_{hydr.}$ (nm)	Detected (%)	$r_{hydr.}$ (nm)	Detected (%)	$r_{hydr.}$ (nm)	Detected (%)
Native cells						
2	10–19	100	ND[a]	ND[a]	ND[a]	ND[a]
15–20	13–25	97	88–117	3	ND[a]	ND[a]
50–60	19–37	90	88–146	7	352–675	3
Cell treated with Genistein						
2	17–20	100	ND[a]	ND[a]	ND[a]	ND[a]
15–20	No correlation found					
50–60	27–39	97	161–308	3	ND[a]	ND[a]
Cells treated with Cytochalasin B						
2	12–17	100	ND[a]	ND[a]	ND[a]	ND[a]
15–20	No correlation found					
50–60	27–39	98	161–308	2	ND[a]	ND[a]

[a] ND, not detected.

of Species 2 seen in untreated samples, were related to these fluctuations but they did not cause any significant increase in intensity.

The characteristics of the individual species observed in the FCS measurements are summarized in Table 1. Assuming that the observed large species are aggregates of a large number of small particles, not only an increase of the size but also of the brightness of the particles should be observed. Both parameters characterize the different species. Information about the brightness distribution could not be obtained by FCS but using PCH.

PCH

In Fig. 3, a typical measurement in native cells is shown obtained after 50 min of incubation (orange line). The resulting histogram can be described as contributions from at least three species which is in agreement with the results from FCS measurements. The three species have different concentrations and are discriminated by their brightness values. Concentrations are specified by relative units (r.u.), as the concentration of particles inside the cell is not known. The brightness is specified by counts per second (cps). The following parameters gave the best fit for the measured histograms (Fig. 3): for Species 1 a relative brightness of 1000 cps and a concentration of 350 r.u. were assumed (black line). For Species 2 (red line), and 3 (green line) 2.2×10^6 and 6.0×10^6 cps and relative concentrations of 0.12 and

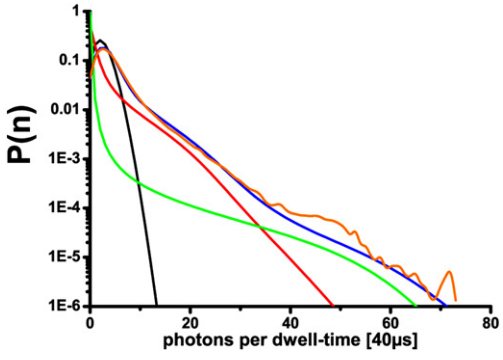

Fig. 3. Simulation of the brightness distribution for three species with different concentration and brightness values. This theoretical and convoluted graph (blue) corresponds to three different species whereas the contribution of every single species is shown in black (Species 1), red (Species 2), and green (Species 3). For comparison to the convolution of these species an experimental curve (orange) is plotted. $P(n)$ represents the probability of detected photon counts. (For interpretation of the references to colors in this figure legend, the reader is referred to the web version of this paper.)

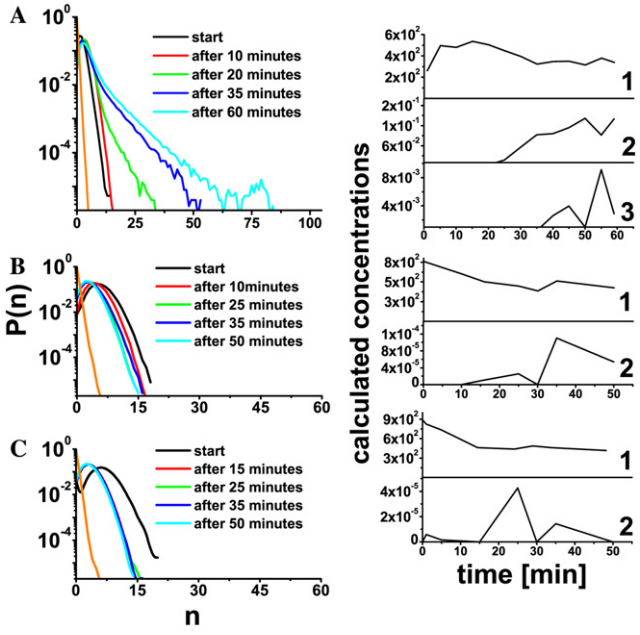

Fig. 4. Normalized distribution of photon counts. Untreated samples (A), cells treated with Genistein (B) or Cytochalasin B (C). On the right side the temporal evolution of the particle-concentration is shown. The numbers in the graphs indicate the particular species. The legends show the different time-points of the measurement. Controls without particles are plotted in orange. (For interpretation of the references to colors in this figure legend, the reader is referred to the web version of this paper.)

0.003 r.u. were proposed respectively. The individual contributions are shown together with their convolution (blue line) which shows good agreement with the PCH measured after 50 min (orange line). These values indicate that the larger species are aggregates of around 2000 (Species 2) and 6000 (Species 3) particles.

These values were used to evaluate the time dependence of appearance of particles in the cytoplasm of a cell (Fig. 4). Species 1 was detected over the whole observation period of 60 min in untreated cells. Their relative concentration changed with time. It increased from an initial value of 261 r.u. to a maximum value of 537 r.u. within about 10 min. Later the relative concentration decreased and stabilized at a value of 339 r.u. after about 20 min. The mean brightness was well defined with 1000 ± 0.8 cps. The decrease in concentration found for Species 1 is accompanied by an increase of Species 2 after about 15 min which reached a final concentration of 0.2 r.u. The respective brightness was calculated to be $(2.2 \pm 0.02) \times 10^6$ cps. Species 3 appeared after about 30 min reaching a relative concentration of 0.003 r.u. with a mean brightness of $(5.8 \pm 0.06) \times 10^6$ cps. This species did not account for a significant decrease of the other two species.

Contrary to untreated cells, in cells treated with Genistein or Cytochalasin B (Figs. 4B and C) only Species 1 was found in significant concentrations. In Genistein treated cells, its relative concentration passed a maximum value (889 r.u. at the beginning) and stabilized at lower concentrations (417 r.u.) similar to untreated cells. The brightness was stable at 1000 ± 0.5 cps. A minute amount of Species 2 with brightness values of $(2.0 \pm 0.5) \times 10^6$ cps and a concentration of 1×10^{-4} r.u. was also observed. In samples treated with Cytochalasin B, the concentration of Species 1 decreased from an initial value of 761–427 r.u. at the end of the measurement (brightness: 1000 ± 0.3 cps). The second species showed brightness values of $(2.1 \pm 0.25) \times 10^6$ cps but a comparably low concentration of 4×10^{-5} r.u.

Discussion

LSM images showed that negatively charged polystyrene particles with a diameter of 20 nm are effectively internalized by human HeLa cells independent of whether the cells were treated with Genistein or not. In native cells, isolated particles and small aggregates were found throughout the cytoplasm. Additionally bright aggregates were found mainly at the periphery of the cell. Such aggregates of individual particles could result from incorporation into endosomes or similar structures (e.g., lysosomes, exosomes, and multivesicular bodies) [26]. In cells treated with Genistein, only small aggregates were found nearer to the cytoplasm membrane. One explanation could be that in that case particles are not efficiently packed into vesicles or that such structures are not actively transported within the cell.

Translocation of particles needs a viable, fluid membrane as particles are not found within dead cells. This is in agreement with earlier results where it was shown that cholesterol depletion, a process which decreases the fluidity of the membrane, reduces the entrance of particles up to 200 nm in diameter [12]. Whereas earlier experiments were performed with fixed cells after long incubation times, it was intended in this study to follow the time-course of the appearance of particles inside the cells under almost physiological conditions. FCS identified highly mobile particles with a hydrodynamic radius of about the size of the applied particles in living cells. Additionally larger species were found at later times with a broad distribution of radii (see Table 1). The appearance of such aggregated species was inhibited if the cells were treated with Genistein or Cytochalasin B. Nevertheless, species showing low brightness values are difficult to detect in the autocorrelation curve if a low number of particles with more than hundredfold brightness are present. Thus, the different species could only be quantified using FIDA (see Figs. 3 and 4).

The photon counting histograms were dominated by a species of rather low brightness, identified as individual 20 nm particles, over the whole observation period independent of the treatment of the cells. In untreated samples, a considerably brighter species accompanied the decrease of the number of individual particles with time. At longer observation times singular events of an even brighter species were observed. In cells treated with cytotoxins aggregation is only detected in minute amounts. The long-term limit of these observations coincides with the results obtained by LSM.

Aggregation must not primarily occur on the surface of the cell but could be the result of active processes within the cell (e.g., internalization of particles within vesicles and their transport). Genistein and Cytochalasin B interact with such aggregation and transport mechanisms [18–21]. However, this aggregation process is time dependent as aggregates within the cell are not observed immediately after addition of particles but with a considerable delay of about 20 min. Even more important is that the used cytotoxins do not inhibit the internalization of singular particles or very small aggregates and their distribution in the cytoplasm. The initial intensities in the PCH measurements indicate that their translocation is even slightly enhanced (Fig. 4) which is in good agreement with recent results obtained in other cell lines [12]. Internalization of such small nanometer sized and negatively charged polystyrene particles is thus not dependent on the availability of active uptake or transport processes, at least in the case of HeLa cells under rather native conditions.

Intracellular aggregation processes like inclusion in vesicles are at least partly responsible for the decrease

of the number of individual particles in the cell. In treated cells, an equivalent decrease occurs even earlier than in native cells and is also more pronounced. As no aggregation is observed in that case it must be concluded that singular particles, initially dispersed over the cytoplasm, are partly released from the interior of such paralyzed cells. This is, however, not due to aggregation as bigger aggregates are not formed and transported within the cytoplasm of treated cells. It is more plausible that the particles leave the cell and are not replaced by new ones due to aggregation and sedimentation processes in the surrounding medium.

As particles can enter the cell without an active uptake it must be assumed that they can also leave the cell easily which could explain the transport of nanoparticles through tissues and even barriers in the body, which normally cannot be overcome by molecular compounds. The molecular mechanisms of this translocation in its context with receptor mediated uptake are currently investigated in detail [11].

Although the experiments show statistical variabilities dependent on the conditions of the individual measurements (e.g., the individual cell or the local particle concentration, due to sedimentation processes), the general pattern for the interaction of particles with cells can be deduced: the used particles penetrate the cellular membrane without a significant delay, endocytotic processes are not necessary for translocation, aggregation occurs at later time and can be blocked by cytotoxins interfering with cellular uptake processes.

Even though the particle concentration used in our investigation, i.e., about 100 $\mu g/10^4$ cells, is very high when compared to particle concentrations in ambient air, which is around 20–50 $\mu g/m^3$ air [27], similar effects could be obtained due to long-term accumulation of inert ultrafine particles in certain organs, e.g., in the alveolae of the lung. The observed mechanisms could thus be responsible for negative health effects of nanoparticles. On the other hand, these results should also contribute to a better understanding of the mechanisms involved in the biotechnological application of nanoparticles as carriers for drugs or DNA.

Acknowledgment

The project is funded by Allgemeine Unfallversicherungs-Anstalt, AUVA, Aldalbert-Stifterstrasse 65, A–1201 Vienna.

References

[1] F. Drewnick, Airborne nanoparticles: properties, measurement and atmospheric relevance, lecture series WS 2004/2005, Max Planck Institute for Chemistry/Exp. Physics.

[2] P. Rajagopalan, F. Wudl, R.F. Schinazi, F.D. Boudinot, Pharmacokinetics of a water-soluble fullerene in rats, Antimicrob. Agents Chemother. 40 (1996) 2262–2265.

[3] M.E. Åkerman, W.C. Chan, P. Laakkonen, S.N. Bhatia, E. Ruoslahti, Nanocrystal targeting in vivo, Proc. Natl. Acad. Sci. USA 20 (2002) 12617–12621.

[4] M.N. Sarbolouki, M. Sadeghizadeh, M.M. Yaghoobi, A. Karami, T. Lohrasbi, Dendrosomes: a novel family of vehicles for transfection and therapy, J. Chem. Technol. Biotechnol. 75 (2000) 919–922.

[5] S. Diabaté, S. Mülhopt, H.R. Paur, R. Wottrich, H.F. Krug, In vitro effects of incinerator fly ash on pulmonary macrophages and epithelial cells, Int. J. Hyg. Environ. Health 204 (2002) 323–326.

[6] J.M. Samet, D.M. DeMartini, H.V. Malling, Do airborne particles induce heritable mutations? Science 304 (2004) 971–972.

[7] K.R. Smith, J.M. Veranth, A.A. Hu, J.S. Lighty, A.E. Aust, Interleukin-8 levels in human lung epithelial cells are increased in response to coal fly ash and vary with the bioavailability of iron as a function of particle size and source of coal, Chem. Res. Toxicol. 13 (2000) 118–125.

[8] S. Boland, A. Baeza-SQuiban, T. Fournier, O. Houcine, M.C. Gendron, M. Chévier, G. Jouvenot, A. Coste, M. Aubier, F. Marano, Diesel exhaust particles are taken up by human airway epithelial cells in vitro and alter cytokine production, Am. J. Physiol. 276 (1999) 604–613.

[9] G. Oberdörster, Z. Sharp, V. Atudorei, A. Elder, R. Gelein, A. Lunts, W. Kreyling, C. Cox, Extrapulmonary translocation of ultrafine carbon particles following whole-body inhalation exposure of rats, J. Toxicol. Environ. Health 65 (2002) 1531–1543.

[10] A. Moore, E. Marecos, A. Bogdanov, R. Weissleder, Tumoral distribution of long-circulating dextran-coated iron oxide nanoparticles in a rodent model, Radiology 214 (2000) 568–574.

[11] G. Oberdörster, Z. Sharp, V. Atudorei, A. Elder, R. Gelein, W. Kreyling, C. Cox, Translocation of inhaled ultrafine particles to the brain, Springer Series on Fluorescence, 2, 2002 154–171, Inhalation Toxicology 16 (2004) 437–445.

[12] J. Rejman, V. Oberle, S.I. Zuhorn, D. Hoeckstra, Size-dependent internalization of particles via the pathway of clathrin- and caveolae-mediated endocytosis, Biochem. J. 377 (2004) 159–169.

[13] N. Kapp, W. Kreyling, H. Schulz, H. Im Hof, P. Gehr, M. Semmler, M. Geiser, Electron energy loss spectroscopy for analysis of inhaled ultrafine particles in rat lungs, Microsc. Res. Tech. 63 (2004) 298–305.

[14] S.T. Hess, S. Huang, A.A. Heikal, W.W. Webb, Biological and chemical applications of fluorescence correlation spectroscopy: a review, Biochemistry 41 (2002) 697–705.

[15] P. Kask, P. Kaupo, D. Ullmann, K. Gall, Fluorescence-intensity distribution analysis and its application in biomolecular detection technology, Proc. Natl. Acad. Sci. USA 96 (1999) 13756–13761.

[16] Y. Chen, J.D. Müller, T.C.S. So, E. Gratton, The photon counting histogram in fluorescence fluctuation spectroscopy, Biophys. J. 77 (1999) 553–567.

[17] J.D. Müller, Y. Chen, E. Gratton, Resolving heterogeneity on the single molecular level with the photon-counting histogram, Biophys. J. 78 (2000) 474–486.

[18] W. Duan, C. Kuo, S. Selvarjan, K.Y. Chua, B.H. Bay, F.S.W.R. Wong, Antiinflammatory effects of Genistein, a tyrosine kinase inhibitor, in a guinea pig model for asthma, Respir. Crit. Care Med. 167 (2003) 185–192.

[19] T. Sorkina, F. Huang, L. Beguinot, A. Sorkin, Effect of tyrosine kinase inhibitors on clathrin-coated pit recruitment and internalization of epidermal growth factor receptor, J. Biol. Chem. 277 (2002) 27433–27441.

[20] J.C. Norman, P.T. Harrison, W. Davis, R.A. Floto, J.M. Allen, Lysosomal routing of Fc gamma RI from early endosomes requires recruitment of tyrosine kinases, Immunology 94 (1998) 48–55.

[21] C. Stournaras, E. Stiakaki, S.B. Koukouritaki, P.A. Theodoropoulos, M. Kalmanti, Y. Fostinis, A. Gravanis, Altered actin polymerization dynamics in various malignant cell types: evidence for differential sensitivity to Cytochalasin B, Biochem. Pharmacol. 52 (1996) 1339–1346.
[22] A.H. Schor, N. Campos, Mechanisms involved in calcium oxalate endocytosis by Madin–Darby canine kidney cells, Braz. J. Med. Biol. Res. 33 (2000) 111–118.
[23] P. Schwille, U. Haupts, S. Maiti, W.W. Webb, Molecular dynamics in living cells observed by fluorescence correlation spectroscopy with one- and two-photon excitation, Biophys. J. 77 (1999) 2251–2265.
[24] S.T. Hess, E.D. Sheets, A. Wagenknecht-Wieser, A.A. Heikal, Quantitative analysis of the fluorescence properties of intrinsically fluorescent proteins in living cells, Biophys. J. 85 (2003) 2566–2580.
[25] P. Kask, C. Eggeling, K. Palo, Ü. Mets, M.Cole M, K. Gall, Fluorescence intensity distribution analysis (FIDA) and related fluorescence fluctuation techniques: theory and practice, in: Ruud Krayenhof, Antonie J.W.G. Visser, Hans C. Gerritsen, (Eds.), Fluorescence Spectroscopy, Imaging and Probes (Springer Series on Fluorescence, 2, 2002) 154–171.
[26] L. Rajendran, K. Simons, Lipid rafts and membrane kinetics, J. Cell Sci. 118 (2005) 1099–1102.
[27] M. Pitz, W.G. Kreyling, B. Holscher, J. Cyruys, H.E. Wichmann, Change of the ambient particle size distribution in East Germany between 1993 and 1999, Atmos. Environ. 35 (2001) 4357–4366.